Long-term evolution of exoplanet systems

Cristobal Petrovich[1,2]

[1]Instituto de Astrofisica, Pontificia Universidad Católica de Chile,
Av. Vicuña Mackenna 4860, 782-0436 Macul, Santiago, Chile.

[2]Millennium Institute for Astrophysics, Chile
email: petrovich.cristobal@gmail.com

Abstract. In this Review, I discuss recent developments on the long-term dynamical evolution of exoplanet systems, focusing on how distinctive dynamical processes may have shaped the orbital architectures of observed populations. I include three applications that highlight part of my own work. First, I examine the high-eccentricity tidal migration of hot Jupiters from a phase of dynamical instability and subsequent secular interactions in two-planet systems. Second, secular chaos as the origin of ultra-short-period planets with extreme period ratios. Third, secular resonance sweeping driven by a dispersing protoplanetary disk as the origin hot Neptunes residing in polar orbits. Finally, I discuss how upcoming observations will allow further constraining the prevalence of these dynamical processes.

Keywords. Planets and satellites: dynamical evolution and stability – Chaos – Planet-disk interactions

---

1. Introduction

The orbital architectures of exoplanet systems is diverse, often displaying vestiges of an active dynamical history. Examples include the population of cold Jupiters in eccentric orbits, hot Jupiters and hot Neptunes in tilted orbits relative to their host's star axis, close-in planets with extreme period ratios, among others (Winn and Fabrycky 2015; Zhu and Dong 2021). As a major goal in exoplanet science we aim to describe the history of these intricate systems and shed light on the relevant mechanisms that shaped their orbits and those that may have taken place in the Solar System.

In this review, I describe two classes of long-term dynamical processes and how they may account for the architectures of different exoplanet populations, highlighting my own work:

(1) *Dynamical instabilities* in multi-planet systems whose long-term evolution reduces the number of planets due to collisions and/or ejections. The remaining planets could reach relaxed, though dynamically excited, states that evolve secularly and lead to tidal decay after their eccentricities reach large values. Possible end results of this evolution path are the *hot Jupiters* (§2, Petrovich 2015) and the *ultra-short-period planets* (§3, Petrovich et al. 2019).

(2) *Sweeping secular resonances* due to gradual changes in the frequencies of the systems' secular modes leading to crossings of secular resonances and subsequent excitation of large eccentricities and/or inclinations. The driver of these changes could be due to a time-varying external perturbation (e.g., a dispersing protoplanetary disk or a decaying stellar quadrupolar moment) or an internal change in the system (e.g., a migrating planet or planetary engulfment). I discuss a possible end

result of this evolution history that may account for an emerging population of *polar Neptunes* (§4, Petrovich et al. 2020).

As the exoplanet sample with well-characterized orbital architectures continues to increase, we will better constrain the prevalence of these long-term dynamical processes and their conditions to manifest in nature.

2. Hot jupiters from dynamical instabilities

Soon after the discovery of the first gas giant planets by radial velocities, gravitational scattering was recognized as a promising mechanism to explain the observed large eccentricities and the existence of hot Jupiters by tidal captures (Weidenschilling and Marzari 1996; Rasio and Ford 1996). Subsequent population-level studies showed that the eccentricity distribution of the gas giants remaining in the system relaxes to a distribution that reproduces that of the observed cold Jupiters (Chatterjee et al. 2008; Jurić and Tremaine 2008). Similar studies including tidal dissipation found that a significant fraction of systems ($\sim 10\%$) are capable of shrinking the orbit of a gas giant and giving rise to a hot Jupiter (Nagasawa et al. 2008; Beaugé and Nesvorný 2012).

Next, I present my own numerical experiments as they were presented at the Kavli-IAU Symposium 382. Although these results have not been published elsewhere, they are broadly consistent with previous results from Beaugé and Nesvorný (2012).

2.1. Numerical experiments

I present N-body simulations of the evolution of the orbits of giant planets orbiting a solar-type star including extra forces to emulate the effects from tidal dissipation on the planets and relativistic precession (see Appendix A). The planets are assumed to have a Jupiter mass and radius. Planet-star and planet-planet collisions are assumed to result in momentum-conserving mergers with no fragmentation. Collisions are assumed to occur when the distance between two planets (or planet and star) becomes less than the sum of their physical radii.

We choose log of the semi-major axis to be uniformly distributed in the range $3 - 7$ au. Labeling the planets by subscripts i in order of increasing semi-major axis, we impose a minimum initial spacing of the orbits given by

$$\Delta a_{i,i+1} \equiv a_{i+1} - a_i > K R_{H,i,i+1}, \quad \text{where} \quad R_{H,i,i+1} = \left(\frac{M_i + M_{i+1}}{3M_\star}\right)^{1/3} \frac{a_i + a_{i+1}}{2},$$

(1)

where $R_{H,i,i+1}$ is the mutual Hill radius of planets with masses M_i and M_{i+1}. The eccentricities and inclinations are drawn from a Rayleigh distribution with parameters σ_e and σ_i. The parameters can be found in Table 1.

In Figure 1 and Table 1, we show the outcomes of the simulation *3pl-K3*. Most of the systems ($\simeq 95\%$) lead to instability with a set of outcomes involving planetary collisions (C), ejections (E), stellar collisions (S), and hot Jupiter formation (HJ). These simulations have an initial Safronov number for parabolic orbits, defined as

$$\Theta \equiv \left(\frac{2GM_p}{R_p}\right)\left(\frac{a}{GM_\star}\right) \simeq \left(\frac{M_p}{M_J}\right)\left(\frac{M_\odot}{M_\star}\right)\left(\frac{R_J}{R_p}\right)\left(\frac{a}{0.25 \text{ au}}\right),$$

(2)

in the range of $\simeq 10 - 30$ so that close encounters mostly lead to ejections relative to planetary collisions (Ford et al. 2001; Petrovich et al. 2014). These scattering encounters

Table 1. Summary of simulated systems and outcomes.

Name	K	$t_{\max}$ [yr]	$t_{V,pl}$ [yr]	$\sigma_e = \sigma_i$	a [au]	N_{sys}	3 pl. (HJ, inactive)	2 pl. (E, C, S)	1pl (2E)
3pl-K3	3	10^7	0.1	0.01	3-7	1,000	221 (162, 49)	634 (444, 161, 29)	141

Notes: 2 pl. (3 pl.) means that two (three) planets remain in stable orbits for a time $t_{\max}$. C, E, and S stand for planet-planet collisions, planet ejections ($d > 10^5$ AU), and planet collisions with the star. 2E means that two planet ejections occur and HJ stands for hot Jupiter (one planet with $a < 0.1$ AU). All the planets in the simulations have radius R_J.
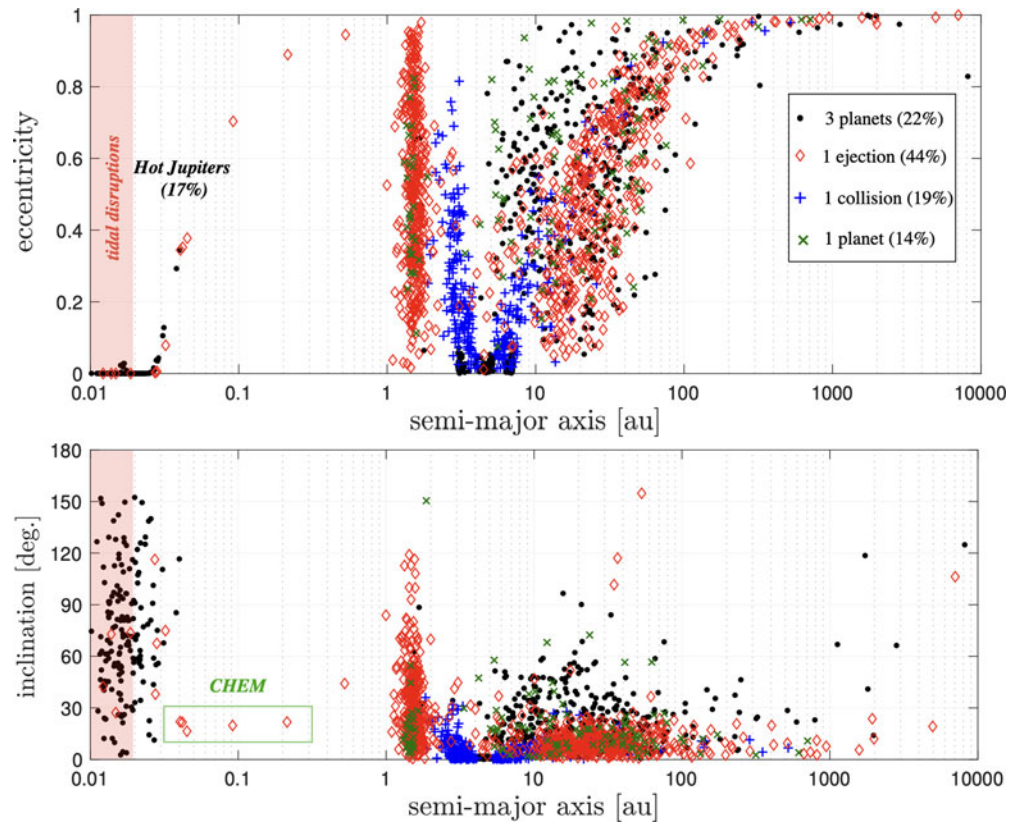

Figure 1. The final orbital elements after 10 Myrs for three-planet systems, where the majority ($\simeq 95\%$) undergoes a phase of strong gravitational scattering. The symbols indicate various outcomes (see Table 1 for more details). A significant population of hot Jupiters is formed, the majority in systems where all 3 planets remain in the system. Note, however, that these planets would have likely been disrupted as their pericenter distances reach inside $\simeq 2R_\odot$ (shaded region in red). In turn, hot Jupiters in two-planet systems tend to circularize to wider orbits, some of which are driven by Coplanar High-eccentricity Migration (CHEM; see green box in lower panel and an example in Figure 2).

are reflected as outcomes involving ejections from the system, collisions with the star, and hot Jupiter formation. Consistently, these outcomes largely dominate relative to collisions.

2.2. *Rate of hot Jupiter formation*

The integrations show that hot Jupiters are formed in $\simeq 17\%$ of the systems. This fraction falls between the $\sim 10\%$ quoted by Beaugé and Nesvorný (2012) and the $\sim 30\%$ from Nagasawa et al. (2008). My HJ rate may be larger than the former because my simulations included only equal-mass planets where the scattering is most efficient. In
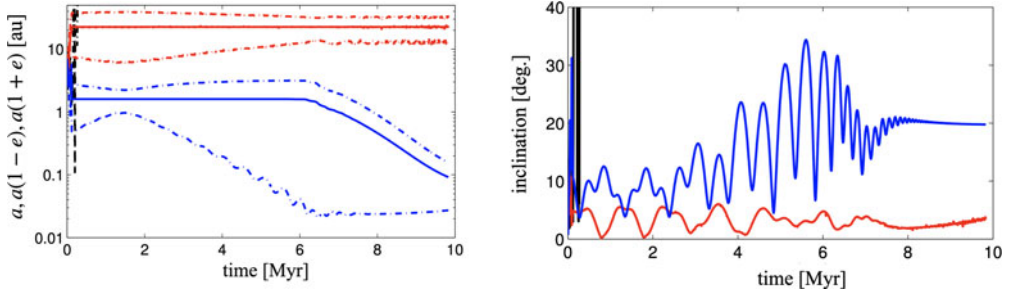
Figure 2. Orbital evolution the planet in the green box of Figure 1, undergoing *Coplanar High-eccentricity Migration* (CHEM; Petrovich 2015). A planet is ejected early on (black line), while the other two relax into a hierarchical configuration ($a_{\rm out}/a_{\rm in} \gtrsim 10$) with eccentric ($e_{\rm in}, e_{\rm out} \gtrsim 0.5$), and mildly inclined orbits ($I_{\rm in}, I_{\rm out} \lesssim 15°$). The subsequent evolution is driven by octupole-level secular perturbations reaching $e_{\rm in} \to 1$ ($a_{\rm in}[1 - e_{\rm in}] \simeq 0.02$ au) after 6 Myrs, time at which the orbits start to lose orbital energy due to tides. On top of the octupole-level cycle, we observe shorter-term quadrupole-level oscillations, most noticeable on the inclinations when the eccentricities are large. The final state of the system would be a hot Jupiter at $a_{\rm in} \simeq 0.04$ au (3-day period) in a circular orbit and an inclination of $\sim 20°$ relative to the initial invariable plane.

turn, these may be lower than the latter, as these authors do not include planetary collisions that reduce the eccentricity excitation and also their efficient prescription for tides that largely prevent collisions with the star (taking place in $\sim 10\%$ of my simulations, mainly as E+S outcomes).

Regardless of the slight discrepancies, the fraction of hot Jupiters in these simulations may not be physical, since none of the above works included the possibility of tidal disruptions when the pericenter distance is $r_p = a(1 - e) \lesssim 2R_\odot$†. Due to the conservation of orbital angular momentum during migration, the final semi-major axis is $a_{\rm final} = a(1 - e^2) \simeq 2r_p$, implying that hot Jupiters with $a_{\rm final} \lesssim 4R_\odot \simeq 0.019$ au would have been disrupted (red-shaded region containing $\sim 70\%$ of the HJs).

2.3. *Coplanar High-eccentricity Migration (CHEM)*

The main outcome from the scattering experiments is the ejection of one planet (red diamonds) leading behind two planets in excited and well-separated orbits. We clearly distinguish an inner planet piled-up at $a_{\rm in} \gtrsim 1$ au as a result of energy conservation, and an outer planet following a track with $a_{\rm out}(1 - e_{\rm out}) \sim 10$ au connecting its orbital path to the region scattering took place. As a result, most of these systems lead to a hierarchical configuration with $a_{\rm out}(1 - e_{\rm out})/a_{\rm in} \sim 5 - 12$.

As recognized in previous work, if these hierarchical systems relax into orbits with large mutual inclinations, then the von Zeipel-Lidov-Kozai (ZLK) mechanism can be triggered and lead to subsequent migration (Nagasawa et al. 2008; Beaugé and Nesvorný 2012). Though this evolution track does happen in some systems, it is not the only possibility. Alternatively, two eccentric planets ($e_{\rm in}, e_{\rm out} \gtrsim 0.5$) with low to moderate mutual inclinations $I_{\rm mut.} \lesssim 20°$ may secularly drive the inner planet to $e_{\rm in} \simeq 1$ and its subsequent migration. A process termed Coplanar High-eccentricity Migration and proposed by Petrovich (2015).

---

† The tidal disruption radius for parabolic orbits is $r_t \simeq 2R_J(M_\star/M_i)^{1/3} \simeq 2R_\odot$ (e.g., Faber et al. 2005).

An example is shown in Figure 2, which corresponds to a system in the green box of Figure 1 (system at $a \sim 0.1$ au, $e \sim 0.7$ and $I \sim 20°$). Here, the dynamics is governed by the following dimensionless interaction potential:

$$\tilde{\phi}_{\text{oct}} = \frac{e_{\text{in}}^2 + 2/3}{2(1 - e_{\text{out}}^2)^{3/2}} - \frac{15}{16} \left(\frac{a_{\text{in}}}{a_{\text{out}}} \frac{e_{\text{out}}}{1 - e_{\text{out}}^2} \right) \frac{e_{\text{in}}(e_{\text{in}}^2 + 3/4)}{2(1 - e_{\text{out}}^2)^{3/2}} \cos \Delta\varpi, \qquad (3)$$

where the second term is the octupole-level coupling responsible for the eccentricity growth. Depending on its amplitude relative to the first quadrupole-level term and the relative apsidal orientations $\Delta\varpi = \varpi_{\text{in}} - \varpi_{\text{out}}$, the inner orbit can reach $e_{\text{in}} \to 1$ (see also Li et al. 2014 for a condition in the test particle limit). The figure shows that this process takes ~ 4 Myr to excite the eccentricity to $e_{\text{in}} \simeq 0.98$, corresponding to the octupole timescale. On top of this, we observe other oscillations that take place in quadrupole timescale due to the nonzero inclinations and become most prominent after ~ 5 Myr when the eccentricity is quite large.

2.4. *The paths to high-eccentricity migration*

Recently, Garzón (2022) performed similar scattering experiments to quantify the relative importance of various eccentricity excitation mechanisms, including secular chaos, CHEM, ZLK oscillations, and a combination of the last two (eccentric and inclined orbits). Their results show that secular excitation from both eccentric (octupole-driven like CHEM) and inclined (quadrupole-driven like ZKL) are most prevalent. In other words, after scattering, the orbits relax to inclined and eccentric orbits as shown in Figure 1. Thus, CHEM operates but generally shows extra inclinations wiggles driven by quadrupole perturbations. Similarly, ZKL typically displays strong octupolar modulations.

We can turn to observations to gauge the leading mechanism, if any. In particular the sky-projected spin-orbit angles λ that have been measured in around 200 systems with short-period gas giants, mainly hot Jupiters. In this sample, the majority has small values of λ, possibly indicative of CHEM or other channels to form hot Jupiters (in situ formation and disk-driven migration). However, such systems may have also started with large λ following other high-eccentricity channels, but have their large tilted damped out by tides (Winn and Fabrycky 2015).

Most recently, measurements of λ have been possible for a more pristine population of warm Jupiters ($a \gtrsim 0.1$ au), which are much less affected by tidal damping of λ compared to hot Jupiters. A notable example is TOI-3362b, a proto HJ with $a \simeq 0.15$ au and $e \simeq 0.7$ that would circularize down to $a(1 - e^2) = 0.07$ au. Espinoza-Retamal et al. (2023a) measured $\lambda = 1.2^{+2.8}_{-2.7}$ deg, indicating with exquisite precision that this migrating planet is well aligned with the host star's equator. As such, the system is most consistent with CHEM with a history similar to that depicted in Figure 2.

3. Ultra-short-period planets from secular chaos

The *Kepler* mission revealed that sub-Neptunes inside ~ 100-day orbits abundantly revolve stars such as the Sun. Although in most systems a single planet is observed to transit, recent works show that this is merely due to geometric selection biases and that the underlying population consists of multiple planets (tipically ~ 3 planets inside ~ 100 days; Zhu and Dong 2021).

Using independent methods to constrain the presence of non-transiting planets, a novel trend arises: *systems with less planets tend to have larger mutual inclinations* (Zhu et al. 2018; He et al. 2020). This trend has been interpreted as indicative of a phase of giant impacts (Hansen and Murray 2013). Much like the case of giant planets discussed above,
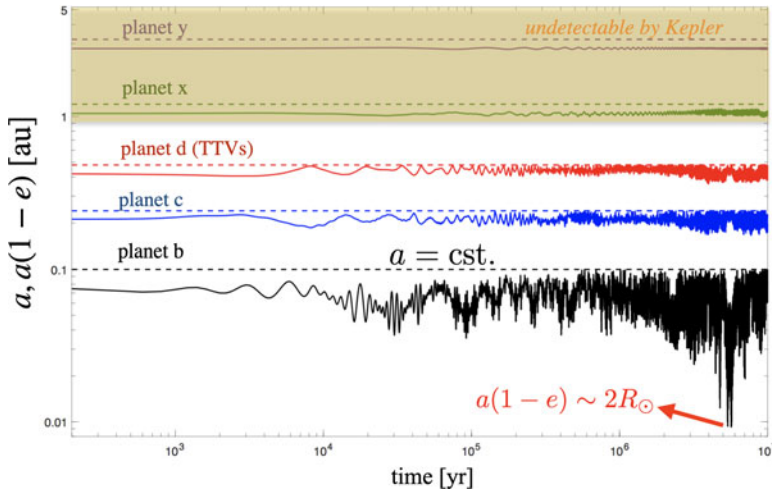
Figure 3. Proposed orbital evolution of the Kepler-10 system from secular chaos that might have led to the tidal migration of planet b from $a_b \sim 0.1$ au down to its current value of 0.016 au from Petrovich et al. (2019). The integration includes planets c and d, and two hypothetical planets (x and y) undetectable by Kepler. The simulation shows the secular and chaotic behavior of the eccentricity of planet b that after ~ 5 Myrs diffuses to large values such that $a_b(1 - e_b) \lesssim$ 0.01 au at which point the orbit can circularize to $a_b(1 - e_b) \lesssim 0.018$ au. The initial eccentricities and inclinations of planets c to y are assumed to be $e = 0.12$ and $i = 7°$, while higher values ($e_b = 0.12$ and $i_b = 7°$) are assumed for Kepler-10b, to speed up its chaotic diffusion. Integrations are carried out with REBOUND-x (Rein and Liu 2012; Tamayo et al. 2020) and include relativistic precession and apsidal precesion from tidal bulges.

these planetary systems may have started with a higher planet multiplicity, and instabilities gradually reduced the number of planets. The main difference is that the Safronov-like number in Equation 2 is significantly reduced compared to that of the gas giants. For a super-Earth with $R_p = 2R_\oplus$ and $M_p = 5M_\oplus$ at 0.2 au, $\Theta \simeq 0.07$. Thus, we expect that instabilities result in planetary collisions, not ejections. As this process repeats, the planets grow and their orbital spacing and 'dynamical temperature' (eccentricities and/or inclinations) also increases (Tremaine 2015).

If the systems indeed settle in these excited states, their long-term orbital evolution may be dictated by secular chaos, much like the evolution of Mercury in our solar system (Laskar 2008). Next, I discuss a possible manifestation of this process in the exoplanet population.

3.1. *Ultra-short-period planets*

Planets with radii between $0.5 - 2R_\oplus$ and periods $\lesssim 1$ days, known as ultra-short-period planets (USPs), represent an extreme planet population. Their equilibrium temperature can exceed $\sim 2000K$ for a Sunlike host, which is hot enough to sublimate dust grains. It has been suggested that, as for hot Jupiters, these planets may have migrated to their locations (Zhu and Dong 2021). Furthermore, the orbits of USPs are also unusual compared to the *Kepler*-like population, as they exhibit significantly larger orbital spacing and higher mutual inclinations (Dai et al. 2018; Petrovich et al. 2019). This orbital architecture suggests a distinctive dynamical past.

A scenario proposed by Petrovich et al. (2019) is that these planets are the end-result of a secular chaos. A scaled-down version in planetary mass and orbital distance of a mechanism proposed for hot Jupiters by Wu and Lithwick (2011). Figure 3 shows an example motivated by Kepler-10 that harbors at least three planets and an extremely

detached USP with $P_c/P_b \simeq 55$. Here, tidal migration due to secular chaos would naturally explain these extreme period ratios starting from a more representative value of $P_c/P_b \sim 4$.

But not all USPs are as extreme as Kepler-10, and their outer neighbors may reside in closer orbits, though still detached. As such, the migration may have started closer to their current orbits without the need of extreme eccentricity excitation. A low-eccentricity excitation model, put forward by Pu and Lai (2019), may fit these systems better.

In either case, the tidal migration provides an explanation for the orbital detachment and also to the increased orbital inclinations that result from these secular interactions and tidal migration.

4. Polar Neptunes from sweeping secular resonances

The long-term evolution of a planetary system can also be influenced by gradual changes in the perturbing potential. Examples include the decaying potential arising from the rotationally induced quadrupolar deformation of a host star (Ward et al. 1976) and that from dispersing protoplanetary disk (Heppenheimer 1980). The time-varying perturbation can gradually modify the secular frequencies of the planetary orbits and lead to passages through secular resonance—a process termed "scanning" or "sweeping" of secular resonances. These passages can drastically increase eccentricities and/or inclinations.

The role and relevance of sweeping secular resonances have been studied in the context of the asteroid belt (Heppenheimer 1980; Lemaitre and Dubru 1991), planet formation through planetesimal accretion (Nagasawa et al. 2005; Best et al. 2023), and even excitation of eccentricities in exoplanet systems (Nagasawa et al. 2003).

In these applications one can simplify the dynamics of the resonance sweeping and reduce it to the second fundamental model of the resonance (Henrard and Lemaitre 1983; Lemaitre and Dubru 1991):

$$\mathcal{H} = -3\Delta(t)R + R^2 - 2\sqrt{2R}\cos(r), \tag{4}$$

where $R \propto 1 - \sqrt{1-e^2} \simeq e^2/2$ (or $R \propto [1-\cos I] \simeq I^2/2$). The sweeping is encapsulated in the evolution of the resonance distance $\Delta(t)$. Note that most previous works ignore the non-linear term R^2, thus only modeling "passages" through linear resonances and not resonant captures. The application described below shows one of the first applications where this distinction becomes crucial.

4.1. *Polar Neptunes*

A number of measurements of the Rossiter-Mclaughlin effect have recently been carried out for planets smaller than Jupiter. As pointed out by Petrovich et al. (2020), these observations reveal an emerging population of hot Neptunes that reside in nearly polar orbits relative to their host star's equator. I caution that the sample is still small with only 5 members, but so far they outnumber the systems residing in aligned orbits in stars smaller than the Sun (Stefànsson et al. 2022). Also, in 3 of these systems long-period Jovian companions are detected (e.g., HAT-P-11 described in Figure 4).

Using this information, Petrovich et al. (2020) proposed that these two-planet systems could engage in an inclination secular resonance capture driven by a dispersing disk. Thus, the angular momentum deficit

$$\mathcal{A} \equiv M_{\rm in}a_{\rm in}^{1/2}(1 - \cos I_{\rm in}) + M_{\rm out}a_{\rm out}^{1/2}(1 - \cos I_{\rm out}) \,, \tag{5}$$

conserved during this process, and largely stored in the outer orbit, is then significantly stored in the inner orbit as $\cos I_{\rm in} \to 0$.
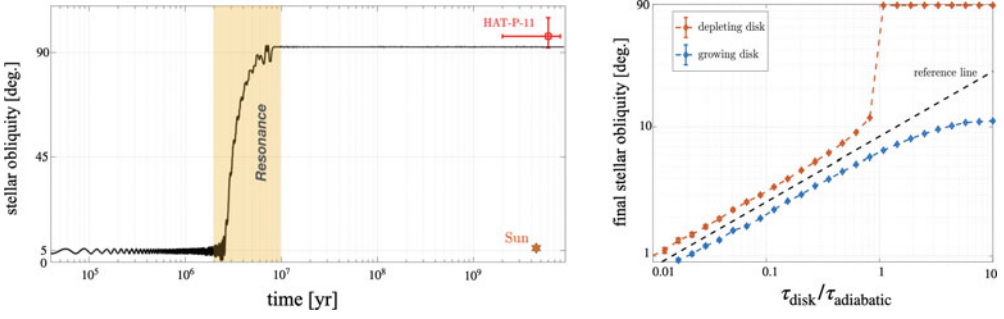
Figure 4. *Left panel*: Evolution of the stellar obliquity relative to the inner planet for a two-planet with parameters (masses, orbital separations) based on HAT-P-11. An initially low obliquity is driven to $\simeq 90°$ during resonance capture after ~ 2 Myrs (shaded region). This evolutionary path would reproduce the observed polar state of HAT-P-11b. *Right panel*: The final stellar obliquity as a function of the adiabaticity parameter $\tau_{\rm disk}/\tau_{\rm adia}$ (see Eq. 7). As expected, polar orbits are only reached when $\tau_{\rm disk}/\tau_{\rm adia} > 1$ (or slowly depleting disks). In order to illustrate the importance of the non-linear term in the resonance model in Equation (4), we include (unrealistic) integrations with a growing disk. Here, the sweep would lead to crossing with $\dot{\Delta} < 0$, not an adiabatic capture. Moreover, this crossing would fall below what is predicted from a linear resonance model due to a non-linear de-tuning (compare to reference dashed line) and saturating at obliquities of $\sim 10°$.

In this work, we reduce the dynamics to the Hamiltonian in Equation (4) with the resonance distance given by

$$\Delta(t) = \frac{2}{3}\left[\frac{1+\eta_\star}{I_{\rm out,0}}\right]^{2/3}\left[1 - \frac{a_{\rm out}^{9/2}}{a_{\rm in}^{3/2}R_{\rm in}^2 R_{\rm out}}\frac{M_{\rm disk}(t)}{(1+\eta_\star)M_{\rm out}}\right], \quad \text{where } \eta_\star = \frac{2J_2 M_\star}{M_{\rm out}}\frac{R_\star^2 a_{\rm out}^3}{a_{\rm in}^5} \tag{6}$$

and the disk of mass $M_{\rm disk}(t)$ has edges at $R_{\rm in}$ and $R_{\rm out}$ (both $> a_{\rm out}$). The star has a quadrupolar moment J_2 and $I_{\rm out,0}$ is the initial inclination of the outer planet. Similarly, we define the adiabatic time scale

$$\tau_{\rm adia} \simeq \frac{2P_{\rm in}}{3\pi}\frac{M_\star}{M_{\rm out}}\frac{a_{\rm out}^3}{a_{\rm in}^3}I_{\rm out,0}^{-4/3}(1+\eta_\star)^{1/3}, \tag{7}$$

such that the resonance capture is guaranteed if the disk dispersal timescale $\tau_{\rm disk} = |d\log M_{\rm disk}/dt|^{-1}$ longer than this. In other words, if the crossing is adiabatic.

In Figure 4 we show the evolution of a system that reproduced the orbital architecture of HAT-P-11, where inner hot Neptune has a nearly polar orbit. A key advantage of this proposal is that high inclinations are achieved starting from small values $\lesssim 5°$. This is simply a result of the much larger angular momentum of the outer orbit compared to that of the inner. The disk only facilitates, quite efficiently, the transfer of angular momentum deficit between the orbits.

Our model relies on a resonance capture, not a simply a crossing event as in most previous studies. To illustrate the importance of this distinction and the role of the nonlinear term R^2 in the dynamics, we included simulations with a range of adiabaticity parameters $\tau_{\rm disk}/\tau_{\rm adia}$ (right panel of Figure 4) and growing and depleting disks. As expected, polar orbits are only reached when $\tau_{\rm disk}/\tau_{\rm adia} > 1$ and for a depleting disk (crossing the resonance with $\dot{\Delta} > 0$). In turn, the unrealistic case of a growing disk would cross the resonance with $\dot{\Delta} < 0$, thus never leading to an adiabatic capture even if $\tau_{\rm disk}/\tau_{\rm adia} \gg 1$. This is a result of the nonlinear resonance detuning and stresses the importance of going beyond the often-used linear secular model which would predict a linear growth of the obliquity with $\tau_{\rm disk}/\tau_{\rm adia}$ (see dashed line as reference).

5. Future prospects

The numerical models presented above have a range of simplifications, ranging from the prescriptions, or absence, of tidal dissipation in the planets and the extent in which the integrations have been carried out. These aspects should be improved upon, and we have the required tools to do so, including new numerical integrators such as REBOUND-x (Tamayo et al. 2020) as well as ring or secular codes to efficiently model the very long-term dynamics (e.g., Sefilian et al. 2023).

Less clear, though, is how to improve our, somewhat arbitrary, choice of initial conditions. For the scattering of giant planets, how many giant planets participate in the scattering process and at what orbital distances? Was there residual gas when the instability ensued? The initial eccentricities, inclinations, and orbital spacing seem less relevant for this application, as the outcomes have little memory of their values after the orbits cross. Some constraints on the initial states of systems with giant planets are becoming possible with the advent of ALMA observations. Examples include direct detections in PDS-70 and indirect means in HD 163296. For the latter, recent work by Garrido-Deutelmoser et al. (2023) showed that combining resonant dynamics with images can place sensitive constraints on their orbital architectures. The subsequent evolution of systems like HD 163296 can dictate the timing of the instabilities.

Finally, a promising venue for moving forward is the better characterization of exoplanet systems. Radial velocity follow-ups with high-precision spectrographs such as ESPRESSO and NEID are pushing the observations of Rossiter-Maclaughlin to smaller planets. We should expect many more measurements of stellar obliquities for warm Neptunes. Moreover, the astrometric measurements from Gaia will likely provide with orbital orientations for cold Jupiters and also information on relative inclinations when combined with TESS data (Espinoza-Retamal et al. 2023b). Thus, opening a new window into the 3D architectures of exoplanet systems.

Appendix A. Numerical integrations of dynamically unstable gas giants

We use the publicly available integration packages of MERCURY6.2 (Chambers 1999). We use use MERCURY's Bulirsch-Stoer (BS) integration algorithm; we justify this choice because we are mostly interested in the evolution of dynamically active systems, where planets experience close encounters, and the BS algorithm handles close encounters better than the other integration algorithms in MERCURY. We include extra forces to model the effects of tides from the host star and general-relativistic apsidal precession due to the host star. These forces are explicitly included in the *mfo-user* routine in MERCURY. The first order post-Newtonian term is given by:

$$\mathbf{f}_{\mathrm{GR}} = -\frac{3G^2 M_\odot^2 a(1-e^2)}{c^2 r^4}\hat{\mathbf{r}}.$$ (8)

For the tides with the host star we consider a prescription for the equilibrium tidal bulge as in Wu and Lithwick (2011), where the acceleration associated with the delayed tidal bulge raised on the planet with mass m_p and radius R_p by the host star is written as:

$$\mathbf{f}_{\mathrm{TD}} = -\frac{GM_\odot^2}{\mu r^2}\left(\frac{R_p}{r}\right)^5 k_{L,p}\left[3 + 9\frac{\mathbf{v}\cdot\hat{\mathbf{r}}}{r}\tau_p\right]\hat{\mathbf{r}},$$ (9)

where $k_{L,p}$ is the Love number of the planet chosen to be 0.52 (polytrope with $n=1$) and τ_p is the planet's time lag, which is related to the planets' viscous time $t_{V,p} = 3(1 + k_{L,p})R^3/(Gm\tau_p)$ (Eggleton et al. 1998). This simple prescription ignores the component of the tidal force that is tangential to the planet's orbital motion, which is equivalent to saying that the planet is rapidly synchronized with its orbital mean motion. Such simplification is justified by the negligible spin angular momentum of the planet relative

to its orbital angular momentum. This prescription also ignores the dissipation inside the star because for the values of τ_p we use, dissipation is dominated by that inside the planet. We ignore the evolution of the spin of the star and, therefore, the effect from the rotational bulges.

References

Beaugé, C. & Nesvorný, D. 2012, Multiple-planet Scattering and the Origin of Hot Jupiters. *ApJ*, 751(2), 119.

Best, S., Sefilian, A. A., & Petrovich, C. 2023, The influence of cold Jupiters in the formation of close-in planets. I. planetesimal transport. *arXiv e-prints*,, arXiv:2304.02045.

Chambers, J. E. 1999, A hybrid symplectic integrator that permits close encounters between massive bodies. *MNRAS*, 304(4), 793–799.

Chatterjee, S., Ford, E. B., Matsumura, S., & Rasio, F. A. 2008, Dynamical Outcomes of Planet-Planet Scattering. *ApJ*, 686(1), 580–602.

Dai, F., Masuda, K., & Winn, J. N. 2018, Larger Mutual Inclinations for the Shortest-period Planets. *ApJL*, 864(2), L38.

Eggleton, P. P., Kiseleva, L. G., & Hut, P. 1998, The Equilibrium Tide Model for Tidal Friction. *ApJ*, 499(2), 853–870.

Espinoza-Retamal, J. I., Brahm, R., Petrovich, C., Jordán, A., & Stefánsson, Guðmundur, e. a. 2023,a The Aligned Orbit of the Eccentric Proto Hot Jupiter TOI-3362b. *arXiv e-prints*,, arXiv:2309.03306.

Espinoza-Retamal, J. I., Zhu, W., & Petrovich, C. 2023,b Prospects from TESS and Gaia to constrain the flatness of planetary systems. *arXiv e-prints*,, arXiv:2309.08665.

Faber, J. A., Rasio, F. A., & Willems, B. 2005, Tidal interactions and disruptions of giant planets on highly eccentric orbits. *Icarus*, 175(1), 248–262.

Ford, E. B., Havlickova, M., & Rasio, F. A. 2001, Dynamical Instabilities in Extrasolar Planetary Systems Containing Two Giant Planets. *Icarus*, 150(2), 303–313.

Garrido-Deutelmoser, J., Petrovich, C., Charalambous, C., Guzmán, V. V., & Zhang, K. 2023, A Gap-sharing Planet Pair Shaping the Crescent in HD 163296: A Disk Sculpted by a Resonant Chain. *ApJL*, 945(2), L37.

Garzón, H. e. a. 2022, Production of hot Jupiter candidates from high-eccentricity mechanisms for different initial planetary mass configurations. *MNRAS*, 517(4), 4986–5002.

Hansen, B. M. S. & Murray, N. 2013, Testing in Situ Assembly with the Kepler Planet Candidate Sample. *ApJ*, 775(1), 53.

He, M. Y., Ford, E. B., Ragozzine, D., & Carrera, D. 2020, Architectures of Exoplanetary Systems. III. Eccentricity and Mutual Inclination Distributions of AMD-stable Planetary Systems. *AJ*, 160(6), 276.

Henrard, J. & Lemaitre, A. 1983, A Second Fundamental Model for Resonance. *Celestial Mechanics*, 30(2), 197–218.

Heppenheimer, T. A. 1980, Secular resonances and the origin of eccentricities of Mars and the asteroids. *Icarus*, 41(1), 76–88.

Jurić, M. & Tremaine, S. 2008, Dynamical Origin of Extrasolar Planet Eccentricity Distribution. *ApJ*, 686(1), 603–620.

Laskar, J. 2008, Chaotic diffusion in the Solar System. *Icarus*, 196(1), 1–15.

Lemaitre, A. & Dubru, P. 1991, Secular Resonances in the Primitive Solar Nebula. *Celestial Mechanics and Dynamical Astronomy*, 52(1), 57–78.

Li, G., Naoz, S., Kocsis, B., & Loeb, A. 2014, Eccentricity Growth and Orbit Flip in Near-coplanar Hierarchical Three-body Systems. *ApJ*, 785(2), 116.

Nagasawa, M., Ida, S., & Bessho, T. 2008, Formation of Hot Planets by a Combination of Planet Scattering, Tidal Circularization, and the Kozai Mechanism. *ApJ*, 678(1), 498–508.

Nagasawa, M., Lin, D. N. C., & Ida, S. 2003, Eccentricity Evolution of Extrasolar Multiple Planetary Systems Due to the Depletion of Nascent Protostellar Disks. *ApJ*, 586(2), 1374–1393.

Nagasawa, M., Lin, D. N. C., & Thommes, E. 2005, Dynamical Shake-up of Planetary Systems. I. Embryo Trapping and Induced Collisions by the Sweeping Secular Resonance and Embryo-Disk Tidal Interaction. *ApJ*, 635(1), 578–598.

Petrovich, C. 2015, Hot Jupiters from Coplanar High-eccentricity Migration. *ApJ*, 805(1), 75.

Petrovich, C., Deibert, E., & Wu, Y. 2019, Ultra-short-period Planets from Secular Chaos. *AJ*, 157(5), 180.

Petrovich, C., Muñoz, D. J., Kratter, K. M., & Malhotra, R. 2020, A Disk-driven Resonance as the Origin of High Inclinations of Close-in Planets. *ApJL*, 902(1), L5.

Petrovich, C., Tremaine, S., & Rafikov, R. 2014, Scattering Outcomes of Close-in Planets: Constraints on Planet Migration. *ApJ*, 786(2), 101.

Pu, B. & Lai, D. 2019, Low-eccentricity migration of ultra-short-period planets in multiplanet systems. *MNRAS*, 488(3), 3568–3587.

Rasio, F. A. & Ford, E. B. 1996, Dynamical instabilities and the formation of extrasolar planetary systems. *Science*, 274, 954–956.

Rein, H. & Liu, S. F. 2012, REBOUND: an open-source multi-purpose N-body code for collisional dynamics. *A&A*, 537, A128.

Sefilian, A. A., Rafikov, R. R., & Wyatt, M. C. 2023, Formation of Gaps in Self-gravitating Debris Disks by Secular Resonance in a Single-planet System. II. Toward a Self-consistent Model. *ApJ*, 954(1), 100.

Stefànsson, G., Mahadevan, S., Petrovich, C., Winn, J. N., Kanodia, S., & Millholland, S. C. e. a. 2022, The Warm Neptune GJ 3470b Has a Polar Orbit. *ApJL*, 931(2), L15.

Tamayo, D., Rein, H., Shi, P., & Hernandez, D. M. 2020, REBOUNDx: a library for adding conservative and dissipative forces to otherwise symplectic N-body integrations. *MNRAS*, 491(2), 2885–2901.

Tremaine, S. 2015, The Statistical Mechanics of Planet Orbits. *ApJ*, 807(2), 157.

Ward, W. R., Colombo, G., & Franklin, F. A. 1976, Secular Resonance, Solar Spin Down, and the Orbit of Mercury. *Icarus*, 28(4), 441–452.

Weidenschilling, S. J. & Marzari, F. 1996, Gravitational scattering as a possible origin for giant planets at small stellar distances. *Nature*, 384(6610), 619–621.

Winn, J. N. & Fabrycky, D. C. 2015, The Occurrence and Architecture of Exoplanetary Systems. *ARA&A*, 53, 409–447.

Wu, Y. & Lithwick, Y. 2011, Secular Chaos and the Production of Hot Jupiters. *ApJ*, 735(2), 109.

Zhu, W. & Dong, S. 2021, Exoplanet Statistics and Theoretical Implications. *ARA&A*, 59, 291–336.

Zhu, W., Petrovich, C., Wu, Y., Dong, S., & Xie, J. 2018, About 30% of Sun-like Stars Have Kepler-like Planetary Systems: A Study of Their Intrinsic Architecture. *ApJ*, 860(2), 101.